Generation of High-Density Electrons Based on Plasma Grating Induced Bragg Diffraction in Air

Liping Shi, Wenxue Li,* Yongdong Wang, Xin Lu, Liang'en Ding, and Heping Zeng†

State Key Laboratory of Precision Spectroscopy, East China Normal University, Shanghai 200062, China

(Received 3 June 2011; published 23 August 2011)

Efficient nonlinear Bragg diffraction was observed as an intense infrared femtosecond pulse was focused on a plasma grating induced by interference between two ultraviolet femtosecond laser pulses in air. The preformed electrons inside the plasma grating were accelerated by subsequent intense infrared laser pulses, inducing further collisional ionization and significantly enhancing the local electron density.

DOI: 10.1103/PhysRevLett.107.095004 PACS numbers: 52.50.Jm, 41.75.Jv, 52.20.Fs, 52.38.Kd

Multiphoton ionization and subsequent electron-ion interaction [1–3] induced by intense ultrashort laser pulses play important roles not only in highly nonlinear and ultrafast processes of atoms and molecules, such as high harmonic generation [4], molecular photodissociation [5,6], electron localization and recapture in atomic or molecular states [7–10], and acceleration of neutral atoms [11], but also in filamented nonlinear propagation of intense ultrashort laser pulses in transparent media. The electron density was demonstrated to increase with the focused peak intensity before saturation around the clamped peak intensity within the plasma channel [12]. For a single infrared filament in air, the electron density is typically limited below 10^{17} cm^{-3} [13–15]. Nonlinear interaction of multiple infrared femtosecond (fs) filaments could generate plasma gratings [16–20] that may tolerate ultra-high-intensity laser fields beyond the clamped intensity limit for free electron generation and acceleration. Filament interaction has already been used to control high-field direct acceleration of electrons over many centimeters [21], phase-matched enhancement of relativistic third harmonic (TH) generation [22,23], dramatic increase of plasma fluorescence in the interaction region [18,24], and even generation of powerful plasma radiation sources at predetermined remote locations using dual laser pulses [25]. It remains unrevealed whether impact ionization induced by appropriate interacting fs filaments could dramatically increase the electron density and how plasma gratings induced by multicolor laser fields could be spatiotemporally coupled to benefit Bragg diffraction and intensify the spatial periodic modulation depth of the generated plasma density.

In this Letter, we demonstrate that nonlinear interaction of two noncollinearly overlapped UV fs filaments could generate plasma gratings along the spatial interference fringes, where the peak electron density was determined to be $>10^{18}$ cm^{-3}. The UV fs laser pulses could be tightly guided in plasma channels of quite small cores due to their excellent focus abilities and the guided intensity in the plasma grooves was enhanced while UV fs laser pulses could ionize atmospheric molecules with a larger multiphoton ionization rate than infrared pulses, the local electron density was thus enhanced significantly in comparison with that induced by single UV filament or interacting infrared filaments. As additional intense infrared fs laser pulses were focused upon the preformed plasma grating at Bragg diffraction angles, nonlinear Bragg diffraction was observed, which intensified the modulation depth of the plasma density generated by the interacting UV filaments. The local peak electron density was enhanced up to 2×10^{19} cm^{-3} via tight guiding of the incident pulses within the plasma gratings. At such a high electron density, the incident laser pulses could accelerate some preformed electrons to trigger inelastic collisional ionization and considerably increased the peak electron density.

Our experiments are schematically illustrated in Fig. 1(a). Intense fs TH pulses with the pulse energy up to 2 mJ and pulse duration ~100 fs were generated from 800-nm fundamental-wave (FW) pulses of a Ti:sapphire regenerative laser of 40 fs pulse duration and 25 mJ output pulse energy [24]. The generated TH pulses were split into two beams, which were simultaneously focused by a concave mirror ($f = 125$ mm) to produce two noncollinearly crossed UV filaments in air. Each individual filament was about 10 mm in length as the UV pulse energy was 1 mJ per pulse. A microscope (10× microobjective) with a CCD (640 × 512 pixels, 1.3 μm/pixel) was installed on the top

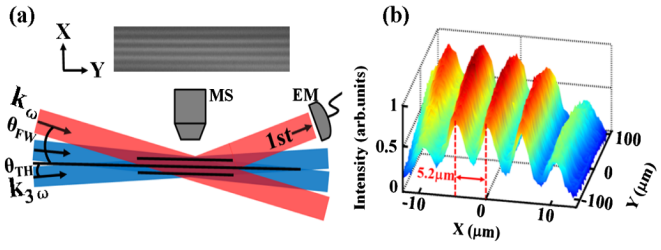

FIG. 1 (color online). (a) Top view of the noncollinear interaction area where two UV filaments interfered to create a plasma grating, with a FW probe beam passing through the interaction region at the Bragg incident angle. 1st: the first-order Bragg diffraction; MS: microscope with CCD; EM: pulse energy meter. (b) Plasma fluorescence distribution from plasma channels induced by the interacting TH femtosecond pulses.

of the filament intersecting region to record the fluorescence image of the plasma channels. As the crossed TH pulses were temporally overlapped in the interaction region, the plasma fluorescence intensity there was observed to exhibit a periodic distribution as shown in Fig. 1(b). The spatial period Λ and effective width D of the periodic fluorescence signal was extracted to be 5.2 and 26.0 μm, respectively. As the plasma fluorescence was closely related with the plasma density, its spatial distribution exhibited a wavelength-scale plasma density modulation, i.e., a plasma density periodically modulated along x axis in the crossing plane with the spatial period determined by $\Lambda = \lambda_{\mathrm{TH}}/(2\sin\theta_{\mathrm{TH}})$ [18], leading to a plasma grating with grooves along the spatial interference fringes (y axis), where θ_{TH} is half of the crossing angle of the TH beams and λ_{TH} denotes the TH wavelength.

The remaining FW pulse after the TH generation was focused by a concave mirror ($f = 500$ mm) onto the preformed plasma grating at the Bragg incident angle $\theta_{\mathrm{FW}} = \arcsin(\lambda_{\mathrm{FW}}/2\Lambda) \sim 4°$, where λ_{FW} denotes the FW wavelength. Figure 2(a) shows the observed far-field light spots of the two TH pulses, the incident FW pulses and their Bragg diffraction, respectively. The zeroth and first order Bragg diffraction of the incident FW pulse were symmetrically located besides two TH beams. Interestingly, spatial intensity interference was established between the FW pulse and its first order Bragg diffraction, giving rise to addition plasma grating induced by the incident FW pulse. At the Bragg incident angle, FW-induced plasma gratings spatially overlapped with the TH-induced ones due to $\Lambda = \lambda_{\mathrm{FW}}/(2\sin\theta_{\mathrm{FW}}) = \lambda_{\mathrm{TH}}/(2\sin\theta_{\mathrm{TH}})$. The Bragg diffraction of the incident FW pulses could thus intensify the UV-induced plasma gratings by further increasing the local plasma density modulation. On the other hand, along the z-axis direction, the interaction region exhibited a thin layer of plasma-induced refractive index change. As the FW pulse was focused on the UV-preformed plasma grating with a diameter larger than the interacting UV filaments, the plasma grating brought about single-slit diffraction with the slit width corresponding to the plasma grating thickness. The FW transmission and single-slit diffraction interfered, resulting in a spatial intensity modulation along the z-axis direction, with three parallel fringes as shown in Fig. 2(b). Such a spatial interference could thus be used to estimate the thickness of the preformed plasma grating. The bright and dark fringes were measured to be $\theta_b = 0.33°$ and $\theta_d = 0.22°$, respectively. The single-slit width d could thus be extracted as $d = \lambda_{\mathrm{FW}}/2(\sin\theta_b - \sin\theta_d) \sim 208$ μm. It was much larger than the UV filament diameter $D = 26$ μm, which implied that the self-projection of the intensity interference fringes of the interacting UV filaments in the x-y plane responsible for plasma grating generation was accompanied with defocusing the incident beams along the z-axis direction. This should be mainly caused by the plasma defocusing effects, evidencing indirectly plasma density enhancement within the plasma grooves.

In order to study the effects of the Bragg incident FW pulses on the preformed plasma gratings, we next measured the Bragg diffraction efficiency at various incident FW pulse energies. For this purpose, a half-wave plate and a Glan laser polarizer were inserted in the FW beam path to vary the incident FW pulse energy. By rotating the half-wave plate to gradually increase the FW energy, the measured diffraction efficiency as a function of the FW energy is shown in Fig. 3 (black curve). The diffraction efficiency in each case of the incident FW energy was scanned to its maximum by tuning the time delay between FW and TH pulses. Interestingly, the Bragg diffraction efficiency increased nonlinearly from 2.4% to 18.7% as the FW energy increased from 0.5 to 10.5 mJ. The observed nonlinear Bragg diffraction were intrinsically originated from the spatially inhomogeneous change of the plasma density due to multiphoton ionization or impact ionization in the presence of intensity interference between the incident and Bragg diffracted FW pulses, which formed local intensity peaks and thus increased the local plasma densities along the UV-preformed plasma grating grooves. As the incident FW pulse energy increased, the plasma density was modulated spatially with an increased modulation depth.

The peak electron density in a single UV fs filament could be roughly estimated as $\rho_e \approx [(0.76 n_2 \rho_c)^K/\sigma_K t_p \rho_N]^{1/K-1}$ [26], where $n_2 \approx 8 \times 10^{-19}$ cm^2/W is the nonlinear Kerr coefficient, $\rho_c = 1.5 \times 10^{22}$ cm^{-3} is the critical plasma density driven by the UV pulse at 267 nm, $\sigma_K \approx 3.53 \times 10^{-44}$ s^{-1} cm^8/W^4 is the multiphoton ionization cross section of nitrogen ionization with four photons $K = 4$, and the UV pulse duration was

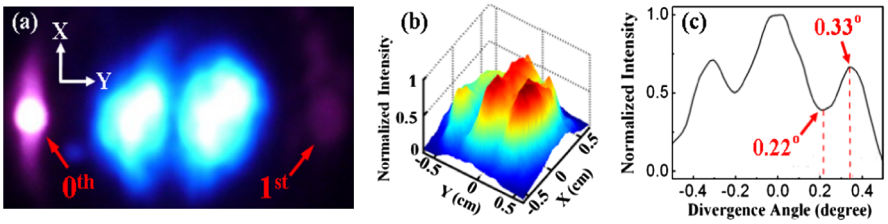

FIG. 2 (color online). (a) Photograph of light spots projected on a white paper screen placed 0.5 m after the filament intersecting point recorded by a digital camera. (b) 3D spatial intensity distribution of the FW beams after passing through the plasma grating. (c) Distribution of laser intensity along y axis after single-slit diffraction from the intersecting filaments.

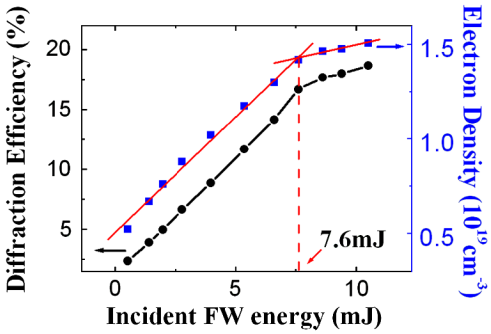

FIG. 3 (color online). Bragg diffraction efficiency induced by plasma grating (black circles) and peak electron density (blue or gray squares) inside the plasma grating versus the incident FW pulse energy.

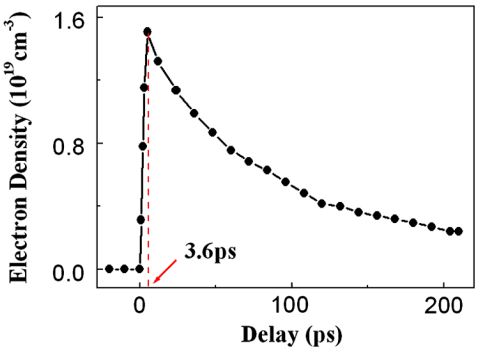

FIG. 4 (color online). Measured peak electron density inside the plasma grating as a function of time delay between the FW and plasma grating forming TH laser pulses.

$t_p \approx 100$ fs. The peak electron density was estimated as $\rho_e \approx 4.6 \times 10^{17}$ cm^{-3}. Experimentally, the peak electron density inside the plasma grating could be determined with the Bragg diffraction efficiency $\eta = \sin^2(\pi \Delta n_p D/\lambda)$ [20], where the refractive index modulation depth is given by $\Delta n_p = -\rho_e/2\rho_c$ according to the simple Drude model. The peak electron densities inside the plasma grating could thus be calculated, as shown in Fig. 3 at versus incident FW energies. As the incident FW pulse was weak, the preformed plasma grating could be probed with negligible influence from Bragg diffraction. For a focused FW pulse energy of 0.5 mJ with the corresponding diffraction efficiency $\eta = 2.4\%$, the refractive index modulation was $\Delta n_p \approx 1.54 \times 10^{-3}$. The peak electron density was estimated to be $\rho_e \approx 5.2 \times 10^{18}$ cm^{-3}, which increased by a factor of 10 as compared to that generated by a single UV filament. Considerable enhancement of electron density was also confirmed by the significant enhancement of fluorescence signal at the filament interaction region.

As the Bragg incident FW laser energy increased, a quick rise of the Bragg diffraction efficiency was observed at low FW pulse energies, and the nonlinear increase became saturated at high FW pulse energies. As shown in Fig. 3, the slope changed towards a slow increase at the characteristic FW pulse energy ~7.6 mJ. The corresponding diffracted energy was measured to be 1.27 mJ. The diffraction efficiency and peak electron density inside the plasma grating were extracted to be $\eta = 16.7\%$ and $\rho_e = 1.4 \times 10^{19}$ cm^{-3}, respectively. The peak electron density in such a case was close to the molecular density in air, indicating nearly complete ionization of air molecules. In comparison with plasma gratings preformed by interfering TH pulses, the plasma fluorescence in the interaction region increased sharply as the Bragg incident FW laser pulses were delayed about 3.6 ps after the TH pulses, and a bright sparking spot could be observed therein. In addition, a blast sound was heard near the geometric focus, while no fluorescence enhancement was observed as the FW pulses propagated ahead of the TH pulses.

We then investigated the plasma decay dynamics by tuning time delay between FW probe and the grating forming TH pulses. The time evolution of the peak electron density inside the plasma channels is shown in Fig. 4, where positive delays refer to probe FW pulse propagating behind the grating forming TH pulses. With the FW pulse energy of 10.5 mJ, the Bragg diffraction efficiency attained its maximum at a delay of 3.6 ps, corresponding to the buildup time of hydrodynamic plasma waveguides with plasma expansion out of the plasma grating grooves. The Bragg incident FW pulses were guided in the plasma grating grooves as the multiphoton ionization induced electrons were expanded out of the grooves, which in turn influenced dramatically the preformed plasma gratings with further ionization. After that, the electron density exhibited a monotonously exponential decay. The plasma lifetime was extracted to be greater than 100 ps.

The dynamic evolution of the plasma gratings excluded direct multiphoton ionization from the FW laser pulses as the main origin for the considerable increase of local peak electron density. A possible mechanism to explain the delayed nonlinear Bragg diffraction is the inelastic collision ionization induced by accelerated ponderomotive free electrons [25]. With a spatially periodic distribution of electrons formed through multiphoton ionization by the interfering UV laser pulses, some of the preformed electrons were further accelerated by the FW electric field. Some accelerated electrons then triggered impact ionization of other molecules and ions, in an avalanchelike process, which induced a sharp increase of electrons. This was confirmed by the plasma fluorescence as observed in Fig. 5. Dramatic enhancement of plasma fluorescence occurred in the interaction region as the Bragg incident FW pulses were appropriately delayed. The Bremsstrahlung emission responsible for the plasma fluorescence background increased dramatically in the UV spectral region, implying that the free electrons in the plasma gratings were accelerated to high energies. Highly ionized nitrogen and oxygen ions were observed, which might be originated from cascade impact

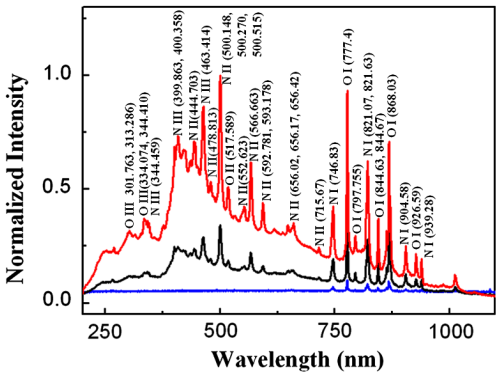

FIG. 5 (color online). Experimentally observed fluorescence spectra from the plasma grating induced by two interfering TH pulses (blue or bottom curve), from plasma grating with a Bragg incident FW pulses of 10 mJ delayed 3.6 ps with respect to the TH pulses (black or middle curve), and from plasma grating with two Bragg incident FW pulses of 5 mJ subsequently delayed 3.6 and 7.2 ps with respect to the TH pulses (red or upper curve), respectively. The emission wavelengths were marked above the corresponding peaks for atomic ions and highly ionized ions. A dramatic increase of plasma and ionic fluorescence indicated impact ionization in the preformed plasma channels.

ionization of nitrogen and oxygen ions after molecular dissociation: $N(O) + e^- = N^+(O^+) + 2e^-$, $N^+(O^+) + e^- = N^{2+}(O^{2+}) + 2e^-$. The accelerated electrons could induce impact ionization of atomic ions only when the ponderomotive energy exceeded their ionization potentials, while the kinetic energy accelerated by the FW pulses could be calculated in eV as $U_p = 9.33 \times 10^{-14} I\lambda^2$ with the FW pulse intensity I in W/cm^2 and the FW wavelength λ in μm [12]. As the accelerated electrons induced efficient impact ionization of N^+ ion, corresponding to the ponderomotive energy $U_p > 29.6$ eV, we could thus estimate a tightly guided FW peak intensity of $I \geq 4.9 \times 10^{14}$ W/cm^2, which is at least 1 order of magnitude higher than the intensity clamping limit [12]. This agreed with recent results [27,28]. As shown in Fig. 5, the ionic spectra and particularly those of highly ionized nitrogen and oxygen ions, increased further with more subsequent Bragg incident FW pulses of appropriate delays. This could be qualitatively understood as follows. The first Bragg incident FW pulse delayed 3.6 ps with respect to the interacting UV pulses were efficiently guided in the plasma grating grooves after appropriate plasma expansion of the preformed plasma grating, accelerating electrons therein to trigger impact ionization that generated an increased electron density in the grating grooves. The second Bragg incident pulse delayed 3.6 ps after the first one accelerated electrons to higher energies, resulting in a dramatic increase of impact ionization, and accordingly more highly ionized nitrogen and oxygen ions were observed.

In summary, we demonstrated nonlinear Bragg diffraction from a plasma grating induced by the interference between two UV fs pulses. The peak electron density inside the plasma grating increased significantly in comparison with that in a single UV fs filament. When an intense infrared pulse was focused on the preformed plasma grating, some electrons were accelerated and inelastic collision ionization generated more electrons, giving rising to a quite high local electron density. A plasma-flare-like radiation source was observed in air. The interaction between several fs filaments could be a promising tool to study nonlinear effects in plasma physics, to control high-order harmonic generation and THz emission, and to compress intense ultrashort laser pulses with wavelength-scale plasma structures.

We acknowledge the support of the National Basic Research Program of China (2011CB808105) and National Natural Science Fund of China (11004061).

*wxli@phy.ecnu.edu.cn
†hpzeng@phy.ecnu.edu.cn

[1] H. Niikura, F. Légaré, R. Hasbani, M. Ivanov, D. Villeneuve, and P. Corkum, Nature (London) **421**, 826 (2003).
[2] V. Bhardwaj, P. Corkum, and D. Rayner, Phys. Rev. Lett. **93**, 043001 (2004).
[3] P. P. Rajeev, M. Gertsvolf, P. B. Corkum, and D. M. Rayner, Phys. Rev. Lett. **102**, 083001 (2009).
[4] M. Lewenstein, Ph. Balcou, M. Yu. Ivanov, A. L'Huillier, and P. B. Corkum, Phys. Rev. A **49**, 2117 (1994).
[5] T. Seideman, M. Yu. Ivanov, and P. B. Corkum, Phys. Rev. Lett. **75**, 2819 (1995).
[6] E. Constant, H. Stapelfeldt, and P. B. Corkum, Phys. Rev. Lett. **76**, 4140 (1996).
[7] M. F. Kling, Ch. Siedschlag, A. J. Verhoef, J. I. Khan, M. Schultze, Th. Uphues, Y. Ni, M. Uiberacker, M. Drescher, F. Krausz, and M. J. J. Vrakking, Science **312**, 246 (2006).
[8] K. P. Singh, F. He, P. Ranitovic, W. Cao, S. De, D. Ray, S. Chen, U. Thumm, A. Becker, M. M. Murnane, H. C. Kapteyn, I. V. Litvinyuk, and C. L. Cocke, Phys. Rev. Lett. **104**, 023001 (2010).
[9] M. Kremer, B. Fischer, B. Feuerstein, V. L. B. de Jesus, V. Sharma, C. Hofrichter, A. Rudenko, U. Thumm, C. D. Schröter, R. Moshammer, and J. Ullrich, Phys. Rev. Lett. **103**, 213003 (2009).
[10] S. N. Pisharody and R. R. Jones, Phys. Rev. Lett. **91**, 203002 (2003).
[11] U. Eichmann, T. Nubbemeyer, H. Rottke, and W. Sandner, Nature (London) **461**, 1261 (2009).
[12] A. Couairon and A. Mysyrowicz, Phys. Rep. **441**, 47 (2007).
[13] F. Théberge, W. Liu, P. T. Simard, A. Becker, and S. L. Chin, Phys. Rev. E **74**, 036406 (2006).
[14] S. Eisenmann, A. Pukhov, and A. Zigler, Phys. Rev. Lett. **98**, 155002 (2007).
[15] Y.-H. Chen, S. Varma, T. M. Antonsen, and H. M. Milchberg, Phys. Rev. Lett. **105**, 215005 (2010).
[16] X. Yang, J. Wu, Y. Peng, S. Yuan, and H. Zeng, in *Proceedings of CLEO 2008 Technical Conference* (Optical Society of America, San Jose, 2008), CTuE6.

[17] H. Wu, T. Yang, Y. Wang, and L. Ding, J. Opt. Soc. Am. B **26**, 645 (2009).
[18] X. Yang, J. Wu, Y. Peng, Y. Tong, P. Lu, L. Ding, Z. Xu, and H. Zeng, Opt. Lett. **34**, 3806 (2009).
[19] X. Yang, J. Wu, Y. Tong, L. Ding, Z. Xu, and H. Zeng, Appl. Phys. Lett. **97**, 071108 (2010).
[20] S. Suntsov, D. Abdollahpour, D. G. Papazoglou, and S. Tzortzakis, Appl. Phys. Lett. **94**, 251104 (2009).
[21] A. G. York, H. M. Milchberg, J. P. Palastro, and T. M. Antonsen, Phys. Rev. Lett. **100**, 195001 (2008).
[22] C.-C. Kuo, C.-H. Pai, M.-W. Lin, K.-H. Lee, J.-Y. Lin, J. Wang, and S.-Y. Chen, Phys. Rev. Lett. **98**, 033901 (2007).
[23] X. Yang, J. Wu, Y. Peng, Y. Tong, S. Yuan, L. Ding, Z. Xu, and H. Zeng, Appl. Phys. Lett. **95**, 111103 (2009).
[24] Y. Wang, Y. Zhang, P. Chen, L. Shi, X. Lu, J. Wu, L. Ding, and H. Zeng, Appl. Phys. Lett. **98**, 111103 (2011).
[25] Z. Henis, G. Milikh, K. Papadopoulos, and A. Zigler, J. Appl. Phys. **103**, 103111 (2008).
[26] A. Couairon and L. Bergé, Phys. Rev. Lett. **88**, 135003 (2002).
[27] P. P. Kiran, S. Bagchi, S. R. Krishnan, C. L. Arnold, G. R. Kumar, and A. Couairon, Phys. Rev. A **82**, 013805 (2010).
[28] P. P. Kiran, S. Bagchi, C. L. Arnold, S. R. Krishnan, G. R. Kumar, and A. Couairon, Opt. Express **18**, 21 504 (2010).